Materials Chemistry and Physics 123 (2010) 776–785

Contents lists available at ScienceDirect

Materials Chemistry and Physics

journal homepage: www.elsevier.com/locate/matchemphys

Synthesis and electrical, spectroscopic and nonlinear optical properties of cobalt molecular materials obtained from PcCo(CN)L (L = ethylenediamine, 1,4-diaminebutane, 1,12-diaminododecane and 2,6-diamineanthraquinone)

O.G. Morales-Saavedra[a,*], M.E. Sánchez-Vergara[b], A.A. Rodríguez-Rosales[a], R. Ortega-Martínez[a], A. Ortiz-Rebollo[c], B.A. Frontana-Uribe[d], V. García-Montalvo[e]

[a] Lab. of Nonlinear Optics, Centro de Ciencias Aplicadas y Desarrollo Tecnológico, Universidad Nacional Autónoma de México, CCADET-UNAM, Apdo, Postal 70-186, C.P. 04510 Coyoacán, Cd. Universitaria, México D. F., Mexico
[b] Coordinación de Ingeniería Mecatrónica, Facultad de Ingeniería, Universidad Anahuac del Norte, Avenida Universidad Anahuac 46, Col. Lomas Anahuac, 52786 Huixquilucan, Estado de México, Mexico
[c] Instituto de Investigaciones en Materiales, Universidad Nacional Autónoma de México, IIM-UNAM, A.P. 70-360 Coyoacán, 04510 México D. F., Mexico
[d] Centro Conjunto de Investigación en Química Sustentable UAEM-UNAM Km. 14.5, Carretera Toluca-Atlacomulco, C.P. 50200 Toluca, Estado de México, Mexico
[e] Instituto de Química, Universidad Nacional Autónoma de México, Circuito Exterior, Ciudad Universitaria, México D. F. 04510, Mexico

ARTICLE INFO

Article history:
Received 9 June 2009
Received in revised form
18 November 2009
Accepted 21 May 2010

Keywords:
Phthalocyanines
Molecular materials
Thin films
Optical materials

ABSTRACT

Novel PcCo(CN)L monomeric complexes were synthesized from $[PcCoCN]_n$ compounds and bidentate axial ligands (L) such as ethylenediamine, 1,4-diaminebutane, 1,12-diaminedodecane and 2,6-diamineanthraquinone. These complexes were implemented to fabricate pellets and thin films by the vacuum thermal evaporation technique. The obtained compounds and deposited thin films were characterized by different spectroscopic techniques. Measurements of the electrical conductivity and the electrical current as a function of temperature were also carried out. IR-spectroscopy studies showed that the ligand attaches to the $[PcCoCN]_n$ unit. The C═N vibrational band is found in the PcCo(et)CN and PcCo(bu)CN molecular solids, although it is displaced with respect to other reported values. Compounds $PcCo(do)_2$ and $PcCo(an)_2$ do not show C═N vibrational bands. This fact suggests a double bond between the ligand and the macrocycle and a coordination at the fifth and sixth position on the Co(III) atom. UV–vis spectra of the thin films exhibited higher conjugation degree for the CN-based samples. Electrical conductivity for the $PcCo(an)_2$ complex was consistently low for all temperature ranges under measurement, whereas the other synthesized compounds showed a semiconductor-like dependence of electric current with temperature. Additionally, cubic nonlinear optical (NLO) characterizations of the film samples were performed with the Z-Scan and third harmonic generation (THG) techniques, all samples exhibit outstandingly high nonlinear activity.

1. Introduction

Phthalocyanine compounds have received a great deal of attention for quite some time because of their semiconductivity and chemical stability [1,2]. In addition, phthalocyanines have the advantage of being very stable against thermal decomposition and show a very intense optical absorption in the visible region [2]. They also have the potential to serve as active materials for molecular electronic devices such as electrochromic displays [3] and optical data storage [4]. In particular, metallic phthalocyanines have been employed to produce low-dimensional conductive materials upon oxidation [5]. Moreover, molecular conductors have been developed by modifying the ligand and the metal ion present in the core of the molecules [6,7]. For instance, the introduction of axial coordinated ligands to the central metal atom has a strong influence on the π-electron conjugation of the macromolecule. Furthermore, the axial substitution exhibits several effects, such as modifying the electronic structure of the phthalocyanine and varying the spatial relationship between neighboring molecules via steric effects and thus, the magnitude of the intermolecular interactions, among others [8]. It has also been observed that large axial coordinated ligands are able to change the packing of the molecules in the solid state and their tendency to aggregate in solution [8]. In addition, it has been noticed that, upon combination of the core metallic ion with a molecular chain, special properties such as the electrical conductivity of a compound can be drastically modified [7,9]. Further interest in phthalocyanine compounds has recently been promoted by the fact that they may be used to formulate molecular materials. These materials generally stack together in a regular way

* Corresponding author. Tel.: +52 55 56 22 86 02x1124; fax: +52 55 56 22 86 37.
E-mail addresses: omar.morales@ccadet.unam.mx, Omar.Morales@daad-alumni.de (O.G. Morales-Saavedra).

0254-0584/$ – see front matter © 2010 Elsevier B.V. All rights reserved.
doi:10.1016/j.matchemphys.2010.05.059

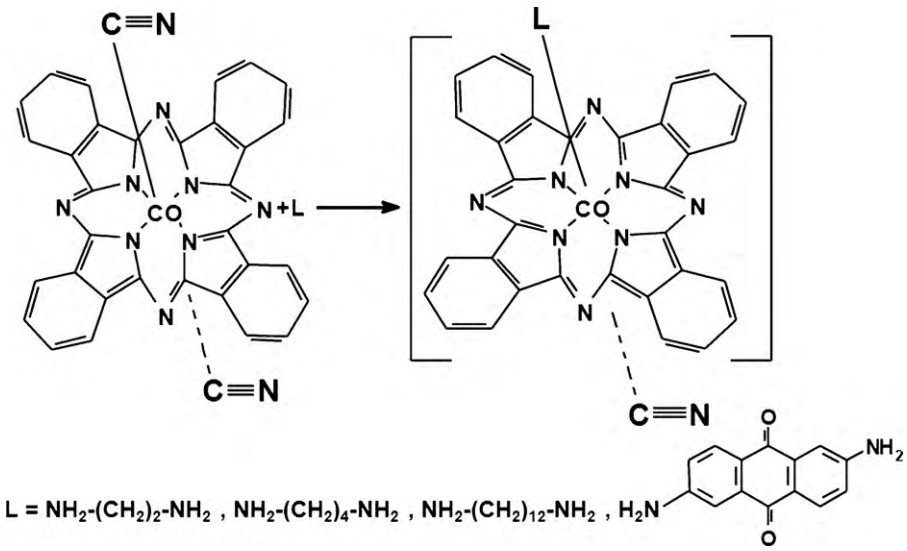

Fig. 1. Chemical structures of the synthesized molecular materials obtained from $[PcCoCN]_n$ compounds (L represents the bidentate amine).

and therefore may exhibit important anisotropic properties. For instance, the electrical conductivity of molecular materials is associated with an extensive delocalization of electrons which depends, in most cases, on the extent of the orbital overlap between molecular units, the planarity, the electronic polarization and the intra and intermolecular vibrations of the molecules, among others [10]. Phthalocyanines are considered ideal building blocks to synthesize molecular materials because they are flat π-conjugated systems bonded to a specific type of central metal which confers them important electrical and photo-physical properties [11,12]. One of the advantages of these systems is that the axial position of the molecule can be easily substituted, leading to multi-dimensional systems with different conductive and optical properties. They may also be employed as active materials in molecular electronic devices such as displays, chemical sensors [3] and optical data storage components [4].

In this paper, we report on the synthesis and photophysical characterization of $[PcCoCN]_n$-based molecular materials. Using bidentate axial ligands (L) such as ethylenediamine, 1,4-diaminebutane, 1,12-diaminedodecane and 2,6-diamineanthraquinone, monomeric PcCoCN(L) and $PcCo(L)_2$ complexes were obtained with different physical properties. These materials were characterized by FTIR, photoluminescent (PL)- and UV–vis spectroscopies, as these molecules show good optical absorbance within the UV–vis region. Furthermore, the electrical conductivity of the compounds in pellets and thin film formats was evaluated as well as the temperature dependence of the electrical current by means of a four-point technique. As observed in inorganic semiconductors, loss of periodicity and crystalline structure results in the localization of electronic wave functions and tail formation in the density of states which extends into the forbidden energy gap at the valence and conduction band edges. Electrical conduction can then be explained from band-theoretical considerations and a hopping model establishing a mobility edge for the charge carriers. Finally, due to their interesting structural conformation and extensive delocalization of electrons, these materials were also evaluated as candidates for cubic NLO effects according to the THG and Z-Scan techniques.

2. Experimental procedure and equipment

2.1. Starting materials and chemicals

All chemicals were reagent-grade from commercial suppliers. (Phthalocyaninate)-cobalt compounds with trivalent central atoms containing cyano groups as axial ligands were produced by adding excess cyanide. The synthesis of (μ-cyano)(phthalocyaninate)cobalt(III), $[PcCoCN]_n$ via splitting off sodium cyanide from sodium dicyano(phthalocyaninate)cobalt(III), $NaPcCo(CN)_2$ was followed according to Metz and Hanack [13].

PcCo(et)CN: 10 ml of ethylendyamine (in excess) were added to 1.0 g (1.8 mmol) of $[PcCoCN]_n$. The new solution was stirred and warmed during 5 days until a deep blue precipitate was obtained which was subsequently filtered, washed with distilled water and absolute ethanol to eliminate the amine and the $[PcCoCN]_n$, respectively, and then dried *in vacuum*. The purified product was obtained by Soxhlet extraction with dichloromethane. Anal. Calcd. For $C_{35}H_{23}N_{11}Co$: C, 64.02; H, 3.51; N, 23.48. Found: C, 64.25; H, 3.12; N, 23.19.

PcCo(bu)CN: 10 ml of 1,4-diaminebutane (in excess) was added to 1.0 g (1.8 mmol) of $[PcCoCN]_n$. The resultant solution was stirred and warmed under reflux for 5 days until a deep blue precipitate was obtained which was subsequently filtered, washed with distilled water and absolute ethanol to eliminate the amine and the $[PcCoCN]_n$, respectively, and then dried *in vacuum*. The purified product was obtained by Soxhlet extraction with dichloromethane. Anal. Calcd. For $C_{37}H_{27}N_{11}Co$: C, 64.91; H, 3.95; N, 22.51. Found: C, 65.06; H, 4.06; N, 22.9.9.

$PcCo(do)_2$: A solution of 0.72 g (0.18 mmol) of 1,12-diaminedodecane (in excess) dissolved in 10 ml absolute ethanol was added to 1.0 g (1.8 mmol) of $[PcCoCN]_n$. This solution was stirred and warmed under reflux for 7 days until a light blue precipitate was obtained which was filtered, washed with absolute ethanol, and then dried *in vacuum*. The purified product was obtained by Soxhlet extraction with dichloromethane. Anal. Calcd. For $C_{56}H_{70}N_{12}Co$: C, 69.35; H, 7.22; N, 17.34. Found: C, 69.15; H, 7.57; N, 16.98.

$PcCo(an)_2$: 1.0 g (1.8 mmol) of $[PcCoCN]_n$ was added to a 15 ml absolute ethanol solution containing 0.86 (1.8 mmol) of 2,6-diamineanthraquinone (in excess). The resultant mixture was stirred and warmed under reflux for 7 days until a blue–green precipitate was obtained. The new complex was then filtered, washed with absolute ethanol, and then dried *in vacuum*. The purified product was obtained by Soxhlet extraction with dimethylformamide. Anal. Calcd. For $C_{60}H_{34}N_{12}O_4Co$: C, 68.9; H, 3.25; N, 16.08. Found: C, 68.21; H, 3.60; N, 15.94.

The synthesis route, starting from the precursor sample up to the generation compounds PcCo(L)CN and $PcCo(L)_2$ is schematically shown in Fig. 1.

2.2. Pellet characterization

KBr pellets of the obtained molecular materials were prepared for basic and reference characterizations. The vibrational spectra of the samples were obtained with a 282-B FTIR Perkin Elmer spectrophotometer. The UV–vis spectra were obtained using a Shimadzu U160 spectrophotometer with methanol, chloroform and acetonitrile solutions. Electrical measurements on pellets were similarly performed as for the thin film samples (see explanation below).

2.3. Thin film deposition and characterization

Thin film deposition of PcCo(CN)L was carried out by vacuum thermal evaporation onto Corning 7059 glass slices and (1 0 0) single-crystalline silicon (c-Si, 200 Ω-cm) wafers. The substrates were kept at 298 K. The Corning 7059 substrates were ultrasonically degreased in warm ethanol and dried in a nitrogen atmosphere. The substrates underwent chemical etching with a p-solution (10 ml HF, 15 ml HNO_3, 300 ml H_2O) in order to remove the native oxide from the c-Si surface. To prevent the powder products from condensing on the surface of the substrate, the

Table 1
Characteristic IR bands (cm^{-1}) of the PcCo(CN)L and $PcCo(L)_2$ based compounds.

Compound	ν(C≡N)	ν(N–H)	$\nu(NH_2)$
PcCo(et)CN (pellet)	2145	–	3070, 2921
PcCo(et)CN (thin film)	2147	–	3069, 2922
PcCo(bu)CN (pellet)	2148	–	3035, 2921
PcCo(bu)CN (thin film)	2150	–	3033, 2922
$PcCo(do)_2$ (pellet)	–	3332	3060, 2920
$PcCo(do)_2$ (thin film)	–	3332	3058, 2922
$PcCo(an)_2$ (pellet)	–	3065	3208, 3334, 3424
$PcCo(an)_2$ (thin film)	–	3063	3208, 3337, 3428
$[PcCoCN]_n$ (pellet)	2142	–	–
$[PcCoCN]_n$ (thin film)	2141	–	–

evaporation source was a molybdenum boat with two grids. The temperature in the boat was 453 K during evaporation, measured with a chromel–alumel thermocouple. It should be remarked that the synthesized compound sublimates. The temperature through the molybdenum boat was slowly increased to 453 K, below the first change observed in the thermo-gravimetric analysis thermogram, to prevent thermal decomposition of the compound.

FTIR-spectra were recorded with a Nicolet 5-MX spectrophotometer with a resolution of 4 cm^{-1}. UV–vis transmission and absorption spectra for films deposited onto naked Corning 7059 glass substrates were obtained within the 200–1100 nm spectral range with a Shimadzu 260 double-beam spectrophotometer, taking air in the reference beam. Photoluminescent spectroscopic measurements were carried out on these samples within the 300–900 nm spectral range with the FluoroMax-3, Jobin-Yvon-Horiba fluorimeter. The excitation wavelengths were selected according to the absorption spectra of the film samples to a convenient wavelength (near the absorption wavelength maximum or at optimal excitation/emission conditions). The thickness of films was determined by ellipsometry using a Gaetner L117 variable-angle manual ellipsometer equipped with a Helium–Neon laser as a light source (λ = 632.8 nm, $\emptyset \sim 1$ mm at 1 mW). The incidence angle was 70°. The infrared and ellipsometric measurements were carried out in films deposited onto c-Si substrates.

The electric conductivity of the films/pellets was studied by means of a four-point probe; for these measurements, the substrates were Corning 7059 glass slices coated with four metallic strips that acted as electrodes. The strips were deposited by thermal evaporation. In order to get an ohmic contact with the deposited films, the electrodes were made from gold or silver. Electric current as a function of temperature was measured with an applied voltage of 100 V in the ohmic regime, using a Keithley 230 programmable voltage source and a Keithley 485 peak-ammeter coupled to an HP3421 data collector.

The surface morphology of films deposited onto glass slices was analyzed by atomic force microscopy (AFM-Park AutoProbe CP equipment), where the acquisition of images was performed in contact mode with an interaction force applied between the sample and the AFM-tip of ~1.5 nN. The AFM system was equipped with a SiN sharpened Microlever™ tip with typical force constant of 0.05 N m^{-1} and resonant frequency of 22 kHz, and this specifies the mechanical characteristics of the used cantilever (typical constants of the instrument).

Finally, the obtained films deposited on Corning 7059 glass slices were also considered as active media for cubic $\chi^{(3)}$-nonlinear optical effects such as THG and nonlinear refraction via the Z-Scan technique. Details of the implemented THG and Z-Scan experimental devices have been recently published in the literature [14,15], where a commercial Q-switched Nd:YAG Laser system (Surelite II from Continuum, λ_ω = 1064 nm, repetition rate of 10 Hz and a pulse width of $\tau \approx 22$ ns) was implemented to provide the fundamental wave for THG experiments. Pulses of energy ~80 μJ were filtered in order to irradiate the samples by means of a f = 50 mm focusing lens, thus peak irradiances on the order of ~3 MW cm^{-2} were achieved at the focal spot on the molecular thin films. This value was below the energy damage threshold supported by the samples under strong focused laser beam irradiation. The polarization of the fundamental beam (S or P polarizing geometry) was selected by means of an IR-coated Glan-Laser polarizer and a λ/2-Quartz-retarder. A second polarizer was used as analyzer allowing the characterization of the THG signals. The third harmonic waves (at $\lambda_{3\omega} \approx 355$ nm) were detected by a sensitive photomultiplier tube placed behind interferential optical filters (centered at 355 ± 5 nm). The THG device was calibrated by means of a fused silica plate ($\chi^{(3)} = 3.11 \times 10^{-14}$ esu, at λ_ω = 1064 nm), which is commonly used as a NLO-reference standard via the Maker-Fringes method [16–18].

On the other hand, the experimental Z-Scan set-up was implemented using an unpolarized laser beam from a 20 mW He–Ne laser system working at 632.8 nm (THORLABS, HRR170-1), this energy was carefully monitored and maintained constant during Z-Scan measurements. The spatial mode of the laser was close to Gaussian TEM_{00}. The polarization plane of the He–Ne laser beam was adjusted and controlled by means of a linear polarizer mounted on a rotatory stage. The polarized laser beam was focused on the sample by means of a positive lens (f = 5 cm), where 9 mW of light reached the studied films. Conversely, the samples were mounted on a motorized translation stage (25 mm length travel in steps of 2 μm) in order to perform Z-Scan experiments. A large area Si-photodetector (EOT ET-2040) was located at ~0.96 m from the focusing lens, after a 1 mm diameter diaphragm aperture. In some experiments a second polarizer was placed in front of the photodetector, in order to analyze polarization components of the transmitted light. All NLO signals captured from photodetectors were measured with a digital oscilloscope (Tektronix TDS, 744A), and finally all motion systems and the administration of the set-ups were automated via a LabView control program.

3. Results and discussion

The $[PcCoCN]_n$ compound was chosen since it is easy to synthesize and because of the cobalt hexacoordination which provides two additional coordination bonds to the molecule that can be coordinated to different ligands. After treating the $[PcCoCN]_n$ compound with the L-molecules such as amines, monomeric PcCo(CN)L and $PcCo(L)_2$ complexes were obtained.

FTIR-spectroscopy studies performed in prepared pellets show that the ligand attaches to the $[PcCoCN]_n$ unit in agreement with Metz and Hanack [13]. The cyano vibrational band in the IR-spectra shows that a strong σ-donor ligand leads to lower values of the cyano band, decreasing the acidity of the central atom while weak σ-donor ligands with π acid properties increase the acidity of the central atom. The IR-spectral features of these compounds are summarized in Table 1. Metz and Hanack [13] observed that, after combining the ligand and the $[PcCoCN]_n$, the IR-spectra showed that the cyano band moves toward a reduction of the σ donant and an increase of the π acceptor from the trans ligands to the cyano group. This phenomenon can be attributed to the Co–C and the C–N bond forces. For instance, the Co–C bond force is mainly determined by the σ-donant capabilities of the cyano ligands. This suggests that a stronger σ donant, trans to the cyano group, lowers the Lewis acidity of the central atom. On the other hand, a weaker σ donant with π-acid properties (acidity-increasing) leads to a shift toward lower values of the cyano band.

From this behavior, the vibrational band of the cyano group provides information about the coordination between the ligand and the metallic ion in the macrocycle. Previous studies [13] suggest that, once the ligand is added to the compound, the C=N vibrational band moves from 2142 to about 2148 cm^{-1}. On the other hand, the absence of this band might indicate a coordination of the ligand with the Co(III) through two molecules in their axial positions. Our results show that the C=N vibrational band is clearly present in the PcCo(et)CN (2145 cm^{-1}) and PcCo(bu)CN (2148 cm^{-1}) molecular solids, although it is displaced with respect to other reported values. This shift may be attributed to the type of ligand employed since no other reports were found on the synthesis of molecular solids with bidentate amines. Compounds $PcCo(do)_2$ and $PcCo(an)_2$ do not show C=N vibrational bands. This fact indicates a double bond between the ligand and the macrocycle, *i.e.*, a coordination at the fifth and sixth position on the Co(III) atom.

Other important bands are the NH_2 band (related to aliphatic amines) located within the 2920–3070 cm^{-1} region and the 2,6-diamineanthraquinone band within the 3208–3424 cm^{-1} spectral interval. All synthesized compounds showed the NH_2 absorption band in their spectra. On the other hand, the presence of the N–H

Table 2
Spectroscopic details of the PcCo(CN)L and PcCo(L)$_2$ based compounds.

Compound	λ (nm)	Band	λ (nm)	Band
PcCo(et)CN	279	N	665	Q
PcCo(bu)CN	279	N	665	Q
PcCo(do)$_2$	279	N	666	Q
PcCo(an)$_2$	281	N	665	Q
[PcCoCN]$_n$	279	N	664	Q

vibrational band may indicate that bidentate amines are coordinated at their ends or that two ligands are coordinated to one single molecule of the cobalt macrocycle. Nucleophilic additions of bidentate amines to metallic macrocycles are related to an infrared absorption band located within the 2954–3372 cm^{-1} region that is associated with a N–H vibration [19–21]. These results are in agreement with those obtained from elemental analysis which indicate that one ligand molecule is present in the PcCo(et)CN and PcCo(bu)CN compounds while two ligand molecules are present in the PcCo(do)$_2$ and PcCo(an)$_2$ based compounds. Moreover, the IR-spectra show the same absorption bands for the thin films as the pristine powders used for evaporation (see Table 1). The slight shifts observed may be due to internal stress produced by the evaporation process. These results strongly suggest that thermal evaporation is a molecular process that does not change the relative chemical composition of the synthesized compounds. Thus, the deposited films are formed by the same macro-ions as those of the original synthesized powders.

The UV–vis optical transmission spectra of different solutions were analyzed within the strong-absorption edge region. Phthalocyanines present two typical absorption bands, namely the Q band in the visible region (600–800 nm) and the B or Soret band in the near-ultraviolet region (300–400 nm) [12,22]. The band at 273 nm is the usual N band of the Pc molecule [12]. It results from the molecular transition $b_{2g}(d_{xy}) \rightarrow b_{1n}(\pi)$. All the compounds have two major absorption bands. The main features of the UV–vis solutions spectra for each synthesized material are summarized in Table 2. The maximum absorption peak in the Q band is assigned to the wavelength-remote region because of the presence of the amine. Since the bidentate ligand may increase the interface distance between macrocycles, the direct π–π orbital overlap is not produced and the Q band remains unchanged. The presence of the absorption band may be interpreted as an overlap of π orbitals through the ligand. It is noted from Table 2 that, except for some minor differences in the N and Q bands, their position is almost the same, regardless of the kind of amine employed.

For thin films deposited on Corning glass slices, some differences in the UV–vis spectra of the solid state samples can be observed as shown in Fig. 2a. The thickness of the deposited films varies from 130 to 430 nm (see Table 3); hence the Beer–Lambert law applies for such semi-transparent thin film systems. It is evident from Fig. 2a, that these films have well defined and relatively different absorptive properties. In general, the weak absorption displayed by all

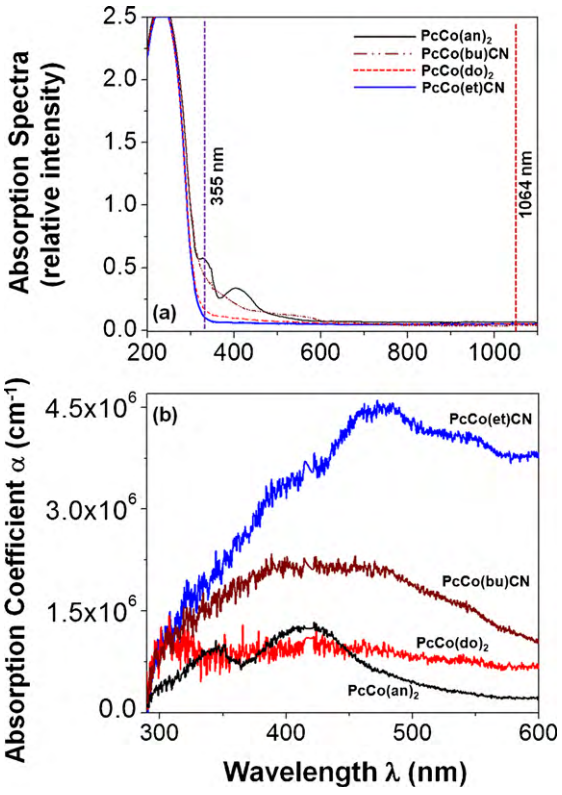

Fig. 2. (a) Comparative absorption spectra of the PcCo(CN)L and PcCo(L)$_2$ based thin film samples deposited on Corning 7059 glass substrates, and (b) spectral evaluation of the corresponding absorption coefficients.

samples within the visible–near infrared (VIS–NIR) range in the thin film format, make these molecular systems attractive candidates for some optical applications due to their appropriate transparency at optical wavelengths. In contrast, higher absorption is detected in the UV region with an absorption peak consistently appearing around 240 nm for all samples; this huge absorption band is produced by the implemented glass substrates.

The main differences observed in the absorption spectra of these samples are properly appreciated within the 300–500 nm interval (see Fig. 2a), where the sample PcCo(bu)CN exhibits low absorption, showing a weak absorption band around 385 nm. Compound PcCo(et)CN exhibits the lowest absorption, showing a smooth and monotonic decreasing behavior. Similarly, compound PcCo(do)$_2$ shows a slightly larger absorption in the same spectral range with the same functional dependence as compound PcCo(et)CN. By contrast, compound PcCo(an)$_2$ exhibits the strongest optical absorption with a different functional dependence. In this case, two well defined absorption bands centered at ~331 and ~405 nm can be easily recognized. Differences on the relative absorption intensities of the studied structures also arise from the diverse grain

Table 3
Thin film thicknesses, electric conductivity and electrical activation energy of the PcCo(CN)L and PcCo(L)$_2$ based compounds at 20 °C with an applied voltage of 100 V.

Compound	Electrical conductivity σ (Ω^{-1} cm^{-1})	Activation energy ΔE_m (eV)	Film thickness (nm)
[PcCoCN]$_n$ (pellet)	2.9E-6	0.103	–
[PcCoCN]$_n$ (thin film)	3.2E-6	0.10	180
PcCo(et)CN (pellet)	8.3E-7	0.08	–
PcCo(et)CN (thin film)	9.9E-7	0.12	150
PcCo(bu)CN (pellet)	6.5E-7	0.077	–
PcCo(bu)CN (thin film)	6.6E-7	0.08	180
PcCo(do)$_2$ (pellet)	5.5E-6	0.109	–
PcCo(do)$_2$ (thin film)	5.9 E-6	0.11	130
PcCo(an)$_2$ (pellet)	1.0E-7	–	–
PcCo(an)$_2$ (thin film)	2.0 E-7	–	430

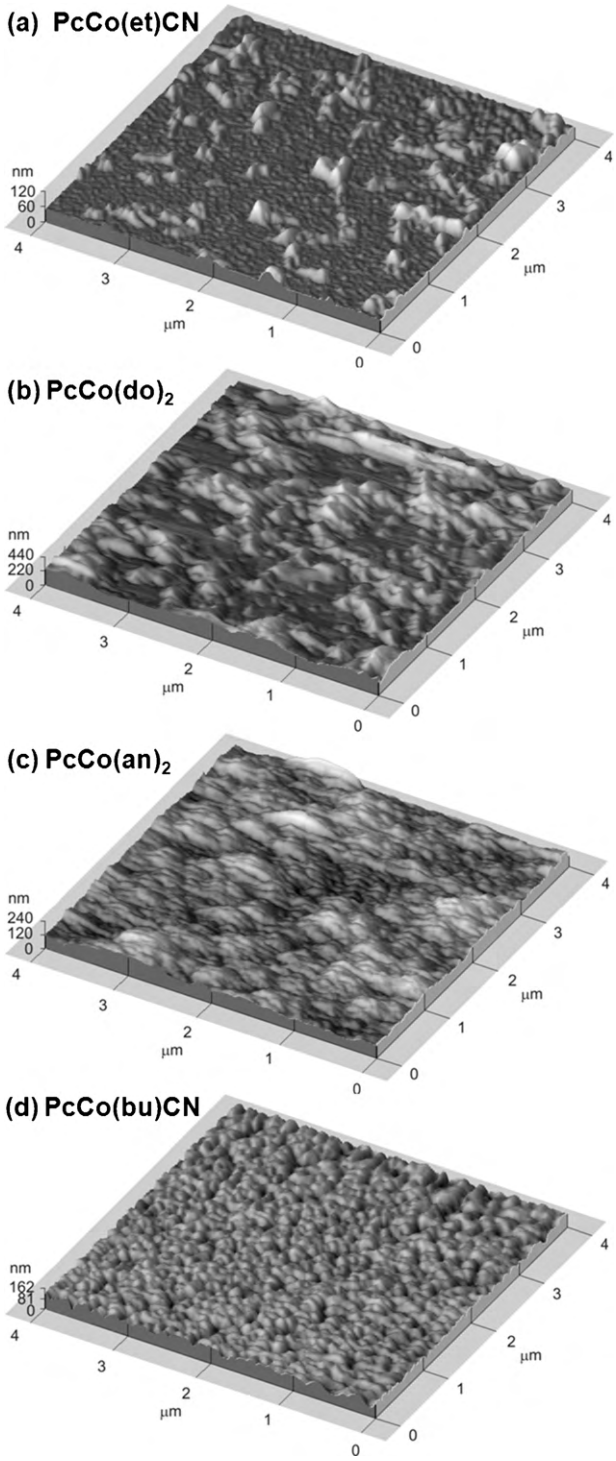

Fig. 3. 3D-micrographs obtained by AFM, showing the surface morphology of thin films deposited on Corning 7059 glass slices from: (a) The PcCo(et)CN sample, (b) sample $PcCo(do)_2$, (c) sample $PcCo(an)_2$ and (d) sample PcCo(bu)CN, respectively.

densities observed by AFM-micrographs (see Fig. 3), where maximal absorption was found for the densely packed $PcCo(an)_2$ based thin film structure, followed by the PcCo(bu)CN and $PcCo(do)_2$ samples. Furthermore, it is observed that the positions of the absorption bands are weakly influenced by the inner backbone structure of these compounds. Finally, the wide and non-negligible absorption band exhibited by the PcCo(bu)CN molecular system (λ = 400–500 nm) and by compound $PcCo(an)_2$ within the visible region (centered at λ = 405 nm), may indicate a larger conjugation degree of delocalized π electrons compared to the other samples, which only exhibits minor absorption tails from this value on. This suggestion will be explored by means of NLO-THG experiments as shown below. Under this context, the available laser excitation line (at λ_ω = 1064 nm) and the line at the THG wavelength ($\lambda_{2\omega} \approx 355$ nm) are also depicted in Fig. 2a. At these wavelengths, non-extreme absorption conditions occur, allowing moderate resonant conditions for cubic NLO characterization. Fig. 2b exhibits the linear absorption coefficients evaluated according to the different film thicknesses (see Table 3) within the 300–600 nm interval, which are very useful for the evaluation of the nonlinear refraction coefficients according to the Z-Scan technique.

The variations in the microscopic morphology and roughness of the films were examined by atomic force microscopy on films deposited onto the Corning glass slices, where 3D-micrographs are exhibited in order to provide an adequate surface inspection (4 μm × 4 μm) of the micro-structural arrays, topological structure, porosity and film quality of the deposited layers as shown in Fig. 3. In general, a homogeneous and acceptable film quality suitable for optical characterizations can be observed for all deposited samples. For the PcCo(et)CN film sample, one can observe small-particle distribution at the film surface (with an average size of ~60 nm, measured from amplified high-quality digitalized images), although some huge and asymmetrical grains with sizes ranging from 100 to 300 nm, regularly distributed on the film surface can be easily distinguished. This may be indicative of a possible nucleation process onset (Fig. 3a). Nonetheless, this sample exhibits the smallest rms rugosity, with a value of ~94.9 Å. In the case of films deposited from $PcCo(do)_2$ and $PcCo(an)_2$ small particles agglomerate to generate larger and rounded or rod-like grains, showing a reasonably homogeneous distribution at large micrometric length-scales with average dimensions of ~300 nm in length (see Fig. 3b and c). These arrangements show the largest roughnesses with smaller inter-grain boundaries; here, at least a bimodal grain-size distribution can be observed. The rms rugosity of these samples is on the order of ~454 and ~234 Å, respectively. Finally, for the PcCo(bu)CN-based film sample, a dramatic change in the film morphology can be observed: agglomeration effects disappear to give rise to a fine surface grain distribution, exhibiting an extraordinarily smooth structure with a regular particle size distribution, here the homogeneity of the film surface suggest optimal deposition conditions for this kind of material, where only formation of smaller and rounded ordered particles with average diameters of ~100 nm can be observed. The rms rugosity of this sample shows an intermediary average value of ~187 Å. These values contribute to an improvement of the film quality obtained for this compound (see Fig. 3d). AFM studies suggest, in general, the formation of regular structures with no drastic variations across the film. In terms of the organic compound used as precursor, the lower rugosity is presented by films of materials obtained from PcCo(et)CN and PcCo(bu)CN, whereas in films obtained from $PcCo(do)_2$ and $PcCo(an)_2$ the rugosity is drastically increased. The rms roughness calculated for these films is an excellent value in reference to the deposition process and for applications in electronic and opto-electronic devices. For the purposes of the present work, it is expected that such morphological variations as observed in the film samples will affect other important photo-physical and NLO properties.

PL-measurements were carried out at room temperature (in air atmosphere) on the same films deposited on glass slices (the excitation wavelength line was set to λ_{ex} = 330 nm) and the PL-spectra were recorded from 350 to 900 nm as is shown in Fig. 4. Based on the fluorescence spectra obtained from the precursor and a Corning 7059 glass substrate (not shown here for simplicity), we consider that the resultant spectra of the studied compounds are constituted from the following PL-peak signals: 375, 397, 452, 470, 482, 493 538, and 581 nm. The bands centered at 397 and 470 nm remain

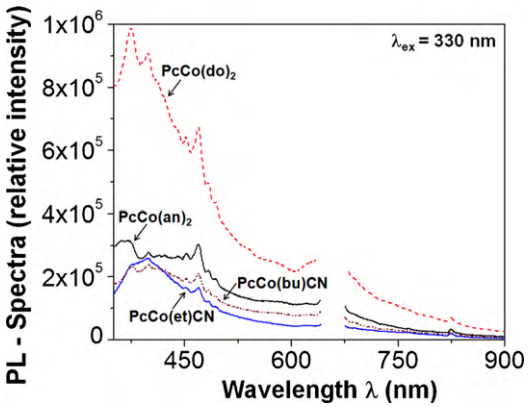

Fig. 4. Comparative PL-spectra recorded in the PcCo(CN)L and PcCo(L)$_2$ based thin films deposited on Corning 7059 glass slices (λ_{ex} = 330 nm).

nearly unchanged showing strong signals for all compounds, whereas all other PL-peaks gradually disappear and/or modify their shape within the PL-spectra of compounds PcCo(bu)CN and PcCo(et)CN. In the present experiments, the main PL-emissions were recorded for all studied samples within the 360–520 nm spectral range. Highest PL-intensity profile was obtained from the PcCo(do)$_2$ sample although its smallest film thickness and absorption coefficient (see Fig. 2b) are indicative of a complex multi-level electronic structure. Weaker PL-emission intensities were found for samples PcCo(an)$_2$, PcCo(bu)CN and PcCo(et)CN, respectively. This behavior is at least partially correlated for samples PcCo(an)$_2$ and PcCo(bu)CN, which show the most interesting absorbance profiles from the optical point of view (see Fig. 2a) and thicker film thickness. Here, we hypothesize that the non-negligible absorption bands observed within the 300–500 nm spectral range for the PcCo(an)$_2$ and PcCo(bu)CN based thin film samples, may decrease the PL-emission (particularly in the case of compound PcCo(bu)CN) within this interval due to strong self-absorption effects induced by the relatively high conjugation degree of this compound. PL-measurements indicate, according to the absorption coefficients, that in the case of the PcCo(bu)CN and PcCo(et)CN samples, most of the energy is thermally dissipated within the material network with poor PL-emissions. This may be suitable for some cubic NLO effects, particularly for Z-Scan measurements. Indeed, nonlinear refraction and absorption strongly depends on the absorptive properties of the materials (both in local and non-local mechanisms [14]), thus according to Fig. 2b, higher NLO-refractive coefficients must be expected for more absorptive samples. Conversely, THG extremely depends on the thickness of the sample, thus higher THG signals are expected for thicker samples with adequate multi-level electronic organizations. These hypotheses were explored by means of NLO measurements as explained below. Another interesting phenomenological observation is the fact that the magnitude of the rms roughness values of the samples is absolutely well correlated to that of the maxima PL-peaks. In fact, higher rugosity produces larger film surface areas and hence a larger number of active surface molecular emitters, which overcome volume self-absorption effects.

Changes in the electrical current were evaluated using the 4-point probe method in the ohmic regime at a constant applied voltage of 100 V for all the synthesized compounds (pellets and film samples). The measurements were carried out on a single line using equal spacing between the acquisition points and small currents to avoid overheating of the samples. The electrical current through the molecular material was measured as a function of temperature. Finally, the electrical resistance and the conductivity were determined. Fig. 5a shows the temperature dependence of the natural logarithm of the electrical current through pellets of

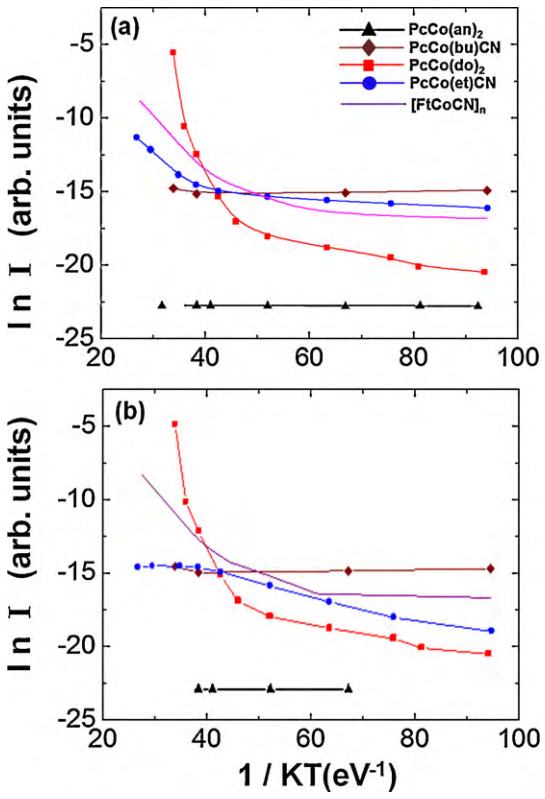

Fig. 5. Natural logarithm of the electrical current as a function of temperature measured in the PcCo(CN)L and PcCo(L)$_2$ based molecular systems for: (a) the pellet samples, and (b) the thin film samples deposited on Corning 7059 glass slices.

the new compounds within the −150 to 170 °C temperature range. The variations observed in the magnitude of electric current may be due to the different amine groups. The PcCo(an)$_2$ complex showed an almost constant behavior in the range of temperatures employed. This may be due to the amine type used as ligand. As this is a compound containing anthraquinone and aromatic groups, the electrical behavior of the amine is characterized by low charge transport. This behavior is different from the one observed in the bidentate ligand and in Ni–Jäger complexes [21]. This suggests that the type of macrocycle that was used and particularly the metallic ion in the complex are decisive factors to account for in charge transport phenomena. The [PcCoCN]$_n$, PcCo(et)CN, PcCo(bu)CN and the PcCo(do)$_2$ plots showed a clear semiconductor behavior as the natural logarithm of the electrical current slightly increased with temperature.

At low temperatures, the PcCo(an)$_2$ sample exhibits the lowest current value, while the PcCo(bu)CN sample shows the largest electrical current. Conversely, at high temperatures, the PcCo(do)$_2$ sample shows the largest electrical current while the PcCo(an)$_2$ sample still exhibits the lowest current value. The electrical-current changes of the compounds suggest that the addition of the ligand to the macrocycle has an influence on the conductivity, especially in the case of ligands with anthraquinone groups, though it is relevant as well in the remaining bidentate amines. Fig. 5b shows the temperature dependence of electric current through thin films during measurements, for a constant applied voltage within the ohmic regime. It may be concluded, similarly to the pellet measurements, that: the PcCo(an)$_2$ complex showed an almost constant behavior in the range of temperatures employed and the [PcCoCN]$_n$, PcCo(et)CN, PcCo(bu)CN and the PcCo(do)$_2$ plots showed a semiconductor behavior.

From these results, the electrical conductivity at room temperature was evaluated for each complex, as well as for the starting

compound. The electrical conductivity σ of these materials depends on the absolute temperature T as described in Eq. (1), and was measured along only one direction.

$$\sigma = \sigma_m \exp\left(-\frac{\Delta E_m}{KT}\right) \quad (1)$$

where σ_m is the pre-exponential factor, ΔE_m is the activation energy for electric conductivity, and K is Boltzmann's constant. Calculated values of ΔE_m are shown in Table 3. The quantity ΔE_m is an activation energy involving both the energy necessary to excite electrons from the localized states toward extended states through the mobility edge and the electrical conduction by means of the hopping mechanism between localized states. The electric conductivity at 298 K for the synthesized molecular solids and the starting materials was also calculated in pellets and thin films (see Table 3). The PcCo(do)$_2$ compound shows electrical conductivity values within the reported intervals found in the literature for molecular semiconductors (from 10^{-6} to 10^{1} Ω^{-1} cm^{-1}) [23,24].

From Table 3, it is observed that all compounds except PcCo(do)$_2$ show an electrical conductivity which is lower than that of the cobalt polymer, although these values are lower than those reported in the literature [13], suggesting that the addition of ligands to the macrocycle decreases the conductivity of the compound. Different approaches [25] have been asserted in order to understand the conductivity of these systems. For instance, Orti [26] suggests that the charge transfer is determined by the π orbitals of the ligand and the orbitals of the metal. On the other hand, from a general point of view, it is believed that charge transfer in these materials occurs via a direct π–π interaction along the stacking of the phthalocyanine rings, in contrast with adjacent phthalocyanines where the interactions are weak. In this case, since the cyano group is absent from the PcCo(do)$_2$ molecule, it is difficult to verify this assumption, although this molecule's conductivity at room temperature is higher than for the PcCo(et)CN and the PcCo(bu)CN complexes, where the cyano group is coordinated to the metallic ion. Nevertheless, phthalocyanines generally exhibit large charge transport in one particular direction, probably due to the columnar stacking of their molecules [27]. Conductivity may be explained in two stages, which can be distinguished from curves I vs $1/KT$ (see Fig. 5a and b) for these compounds: (i) at high temperatures, conductivity is achieved because thermal energy is large enough to excite electrons from the extended sates into the conduction band. Conductivity will be due to the motion of electrons in the electric field. (ii) In the second stage, namely thermally-assisted jump, which occurs at lower temperatures, electrons in localized states may contribute to conductivity only if they acquire enough energy to hop from one localized state to another.

Finally, taking into account the amorphous-close or even an anisotropic (but centrosymmetric) thin film structural arrangement of the synthesized compounds (verified by the absence of quadratic $\chi^{(2)}$-NLO second harmonic generation SHG effects, which necessarily require a crystalline non-centrosymmetric structure), the cubic $\chi^{(3)}$-NLO properties were investigated by means of the optical THG and Z-Scan techniques; measurements were performed in the film structures deposited on glass substrates at room conditions.

According to our Z-Scan device, the NLO response of the developed films was characterized by varying the polarization input planes of the He–Ne laser system in order to explore microscopic material asymmetries or anisotropies throughout the film structure. The observed non-local effect of the samples is shown in Fig. 6a–d, where the nonlinear refractive response of the samples can be unambiguously appreciated by typical peak–valley transmittance curves. One can first recog-

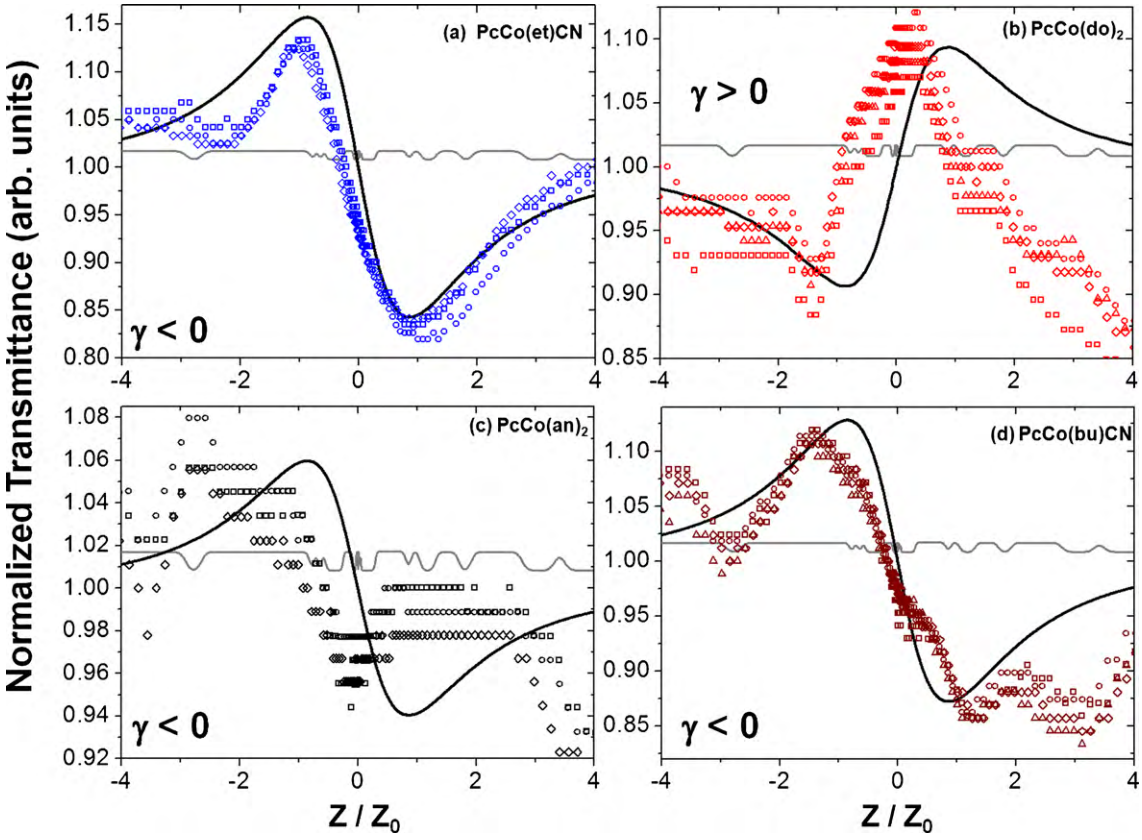

Fig. 6. Z-Scan transmittance curves obtained at different input polarization states (PS: 0–90°) for the PcCo(CN)L and PcCo(L)$_2$ based thin films deposited on Corning 7059 glass slices, exhibiting both negative and positive nonlinear refractive indexes (average theoretical fits TFs and the Z-Scan transmission curve of the reference glass substrate are also included as continuous lines). (a) The PcCo(et)CN sample, (b) sample PcCo(do)$_2$, (c) sample PcCo(an)$_2$ and (d) sample PcCo(bu)CN, respectively.

nize, according to the theory developed by Sheik-Bahae et al. [28–31] that the PcCo(et)CN, PcCo(an)$_2$ and PcCo(bu)CN based samples exhibit negative NLO-refraction coefficients ($\gamma < 0$), with estimated values, as explained below, of $\gamma \approx -1.41 \times 10^{-1}$ esu, $\gamma \approx -1.42 \times 10^{-2}$ esu and $\gamma \approx -7.83 \times 10^{-2}$ esu, respectively. By contrast, the PcCo(do)$_2$ sample is the only one exhibiting a positive NLO-refractive index ($\gamma > 0$) with an estimated value of $\gamma \approx +7.66 \times 10^{-2}$ esu.[1]

In general, since all measurements were systematically performed with different He–Ne input polarization states (from 0° to 90°) and their respective curves are quite similar for each sample, the film structures do not seem to show any significant anisotropic behavior (at least throughout the film depth, in a perpendicular-close laser beam incidence). So far and as mentioned before, this can still be consistent with a regular and homogeneous columnar stacking of their constituting molecules [27], in this case perpendicularly aligned to the substrate surface. However, Z-Scan measurements are not highly sensitive, as the SHG and THG techniques, to detect material anisotropies, especially for symmetric disk-like molecular systems homogeneously stacked in columnar arrangements [14]. The set of Fig. 6a–d also shows the Z-Scan curve for a naked reference glass substrate (continuous gray lines) which exhibit negligible nonlinear refraction compared to the curves of the molecular film samples, at the employed laser power regime. Similarly, the respective theoretical fits to the Z-Scan transmission data (TFs, solid black lines) are also shown for each particular case in Fig. 6a–d. It should be remarked that the stability of the laser source during Z-Scan measurements was practically constant. In order to perform the TFs, according to several previous theoretical studies, the normalized transmittance T_N can be obtained as function of the dimensionless sample position ($x = z/z_0$), where z_0 is the Rayleigh range and z is the Z-Scan laboratory sample position; thus the TFs can be obtained according to the following equation: $T_N \approx 1 + \Delta\Phi_0[4x/(1+x^2)(9+x^2)]$ [28–31]. The phase shift $\Delta\Phi_0$ can be obtained from the ΔT_{p-v} peak to valley experimental transmittance curve and the diaphragm aperture (S) according to: $\Delta\Phi_0 = [\Delta T_{p-v}/0.404(1-S)^{0.25}]$. These equations are well established and have been proved in early Z-Scan works [28–31]. The theoretical restrictions imposed by these formulas in order to apply such expressions at optimal conditions ($|\Delta\Phi_0| < \pi$, $S \approx 20\%$, etc.) are not always fully satisfied in our experimental results due to the large phase shifts and huge measured nonlinearity. However, in most cases (mainly in the case of well defined $\gamma > 0$ or $\gamma < 0$ curves) our results nearly satisfy these conditions and can be fitted according to these formulas. Thus, for comparison purposes and in order to be consistent with the estimation of the γ-values we have assumed its applicability and used these relations in all cases.

For each Z-Scan curve, the well-known relation used to determine the nonlinear refractive index from the phase shift was employed: $\gamma = \lambda\Delta\Phi/2\pi I_0 L_{eff}$ [28–31]; where λ is the wavelength, $\Delta\Phi_0$ the associated phase shift, I_0 is the input beam intensity (at $z = 0$: focal point) and L_{eff} is the effective thickness of the sample [28–31]. The obtained γ-values are rather large, many orders of magnitude larger than those observed for typical glass substrates or for the classical CS_2 standard reference material: $+1.2 \times 10^{-11}$ esu (Z-Scan at $\lambda = 10.6\,\mu m$) or 6.8×10^{-13} esu (DFWM at $\lambda = 532\,nm$) [28,32]. In fact, according to Fig. 2b, Z-Scan measurements are well correlated to the absorption coefficients of the samples: the larger the absorption coefficient of the sample, the stronger the NLO-refraction and absolute γ-values. Hence, samples PcCo(et)CN and PcCo(bu)CN exhibit the strongest NLO-refractive effects. Consistently, the PcCo(do)$_2$ exhibits a very similar γ-value (in magnitude) to the PcCo(bu)CN sample due to the similar absorption coefficient at the implemented He–Ne laser wavelength (see Fig. 2b). Finally, the PcCo(an)$_2$ sample exhibit the smallest absorption coefficient and NLO γ-value.

Samples with small rugosity such as the CN-based molecular films (PcCo(et)CN and PcCo(bu)CN samples) exhibit a homogeneous granular distribution, with smaller grain sizes (see Fig. 3 and analysis thereof). The decrement of the grain size can also help in the understanding of our experimental Z-Scan findings by assuming a high correlation between the morphological film structure and the NLO response [33]. In this case, the vast number of grain boundaries or interfaces present for these samples induces deviation of the atomic bounds between "unitary cells" from their equilibrium positions, which may cause dangling bounds resulting in extra carriers or defects within the film structure. This is a fact of considerable interest, since it has been demonstrated for several crystalline and poly-crystalline thin film samples, that higher carrier density and defects can enhance in principle the nonlinearity of the materials [34–36]. Indeed, these arguments are, in general, well correlated to the fact that the electrical current (see Fig. 5b and analysis thereof) is higher for the CN-based molecular films, providing stronger absorption and energy dissipation of the incident light which give rise to stronger NLO effects such as nonlinear refractive indices.

Finally, experimental single-beam techniques based on THG provide direct access to the complex value of the non-degenerate $\chi^{(3)}(-3\omega;\ \omega,\omega,\omega)$ cubic nonlinear coefficient. The THG-response accounts only for the electronic response, so that the vibrational, orientational, and thermal effects, which may contribute to the overall nonlinear response of the material (as in Z-Scan measurements), are excluded. Fig. 7a and b show the Maker-fringe patterns and the calibrated nonlinear optical $\chi^{(3)}$-coefficients of the studied thin film samples according to the Maker-fringe technique (front-configuration, P/In-P/Out and S/In-P/Out polarizing geometries under moderate resonant conditions, at $\lambda_\omega = 1064\,nm$ and $\lambda_{3\omega} \sim 355\,nm$). In order to evaluate the $\chi^{(3)}$-coefficients, the Maker-fringe patterns were compared to the fringe pattern generated by a 1 mm thick glass substrate (fused silica) used as reference and calibration sample. The Maker-fringe patterns of the molecular film-plus-substrate systems showed an oscillating dependence with increasing incidence angles close to that of the fringes measured for the reference substrate. Nevertheless, the fringes obtained from the reference glass are clearly less intense than those recorded for the molecular films, which indicates relatively stronger THG conversion within the studied samples; the observed phase-shifts and the lack of sharp multi-oscillations in some measurements are due to differences in the material coherence lengths and different samples thicknesses, thus the THG intensity of each sample will not exactly follow the same phase-matching conditions, generating the same oscillating dependence with the medium thickness. Furthermore, the film thickness and relatively strong absorption conditions experienced by the THG waves (for PcCo(et)CN and PcCo(bu)CN samples, see Fig. 2), or the film quality and corresponding scattering effects (for PcCo(an)$_2$ and PcCo(do)$_2$ samples, see Fig. 3), may partially overshadow or distort their respective Maker-fringe patterns. The THG response obtained at nearly normal incidence gives the highest THG conversion efficiency, which permits the relative evaluation of the $\chi^{(3)}$-coefficients. As a direct estimation of the cubic NLO properties of these materials, considering samples under moderate resonant (absorption) conditions, the determination of $\chi^{(3)}$

[1] NLO refractive index in electrostatic units: $n_2\,(esu) = \left(cn_0/40\pi\right)\gamma$ with $[\gamma] \equiv [m^2\,W^{-1}]$.

may be approximated by the following expression [37]:

$$\chi^{(3)\text{-film}} \propto \chi^{(3)\text{-reference}} \left(\frac{2l_c^{\text{reference}}}{\pi}\right)\left(\frac{\alpha/2}{1-e^{-\alpha l_{\text{film}}/2}}\right) \times \left(\frac{I_{3\omega}^{\text{film}}}{I_{3\omega}^{\text{reference}}}\right)^{1/2} \quad (2)$$

where α is the absorption coefficient of the film sample at the third harmonic free-wave, $l_c^{\text{reference}}$ represents the coherence length of the reference material (~6.2 μm), $\chi^{(3)\text{-film}}$ and $\chi^{(3)\text{-reference}}$ are, respectively, the values of the cubic nonlinear coefficients of the film samples and the fused silica plate reference, while $I_{3\omega}^{\text{film}}$ and $I_{3\omega}^{\text{reference}}$ are the peak intensities of the Maker-fringe patterns of both the film sample and the reference plate at optimal phase matching conditions. In this way, the $\chi^{(3)}$ value of a new material relative to the value of the reference standard can be obtained; hence a calibrated result with a high degree of accuracy can be reported.

In principle, THG is possible for all centrosymmetric and amorphous materials and both the film and the glass substrate contribute to the detected THG signal. The focal length of the focusing lens is ~50 mm in order to make the air contribution to the THG signal negligible; these two contributions must be separately identified in order to give a good estimate of the $\chi^{(3)\text{-film}}$ coefficients. Moreover, since the film is deposited only on one side of the substrate, the experimental configuration is asymmetric from a geometrical viewpoint and different relations have been developed in order to fit respectively the 'front' configuration, where the fundamental beam enters the film first, or the 'back' configuration, where the films stays behind the substrate [38–44]. Under this framework, Fig. 7b shows the calibrated $\chi^{(3)\text{-film}}$-coefficients obtained according to Eq. (2) (front configuration). The largest cubic NLO coefficient was evaluated for the PcCo(et)CN-based film sample, followed by the PcCo(bu)CN, PcCo(do)$_2$ and PcCo(an)$_2$ based films, respectively. The THG signals of the compounds are considerably superior to those measured for the reference substrate, and the estimated $\chi^{(3)\text{-film}}$-coefficients are up to three orders of magnitude larger than that of the reference substrate. In this case however, the magnitude of the $\chi^{(3)\text{-film}}$-coefficients can be partially correlated to the film thicknesses since the thicker PcCo(an)$_2$ sample exhibits the smallest THG signal, whereas all other samples show THG intensities according to their respective film thickness. Furthermore, similarly to Z-Scan measurements, THG experiments are remarkably well correlated to the absorption coefficients, film structure (as previously explained) and to the electrical measurements (see Figs. 2, 3, and 5 and Table 3). In fact, the PcCo(bu)CN and PcCo(et)CN have large film thickness and their absorption coefficients reveal relatively higher conjugation degree within the THG-wavelength range; the smaller the grain size of the film structures, the higher THG nonlinearities. Moreover, adequate and complex multi-level electronic transitions as those measured in the PL experiments, are needed.

Regarding the anisotropy of the samples, it is observed that the S-In/P-Out implemented polarizing geometry produced negligible THG signals; we therefore hypothesize that within the material network, no other preferential electronic pathways, perpendicular to the incident polarization state of the fundamental excitation beam, seems to exist. Hence an isotropic (or amorphous-close) molecular organization represents the most feasible structural conformation achieved by the symmetric disk-like molecular systems within all studied film samples, which agrees with Z-Scan measurements. Moreover, since most of the samples exhibit a semiconductor-like behavior, it is reasonable that samples with higher conductivity exhibit stronger electronic-based THG effects than those observed for the CN-based film samples, and that the polarization of the material charge carriers preferentially follows the electric field driving force of the polarized fundamental beam. Consequently, in an isotropic semiconductor material, the electrons will favorably radiate THG waves parallel to the incident laser beam polarization.

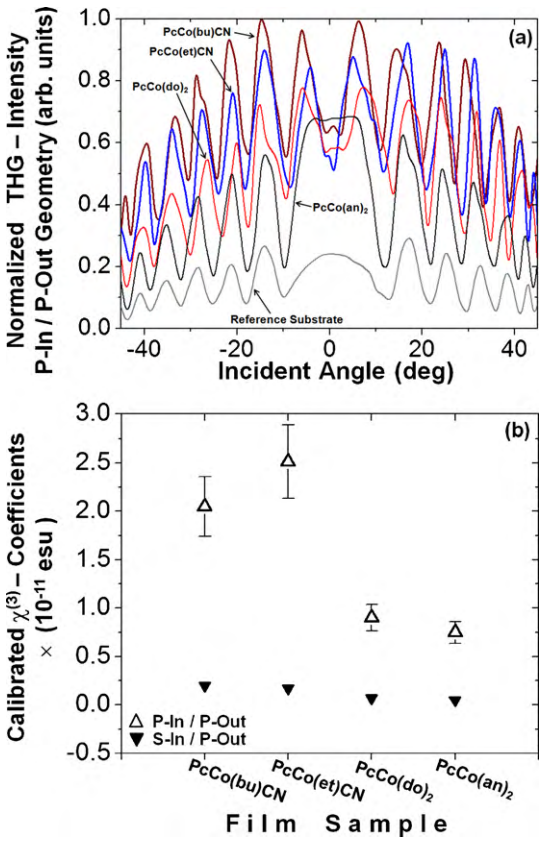

Fig. 7. (a) Angle dependent THG measurement performed in PcCo(CN)L and PcCo(L)$_2$ based thin films deposited on Corning 7059 glass slices (measurements were performed implementing the P-In/P-Out and S-In/P-Out polarizing geometries). (b) Relative calibration of the $\chi^{(3)}(-3\omega;\omega,\omega,\omega)$ NLO coefficients performed according to Eq. (2).

4. Conclusions

In this work [PcCoCN]$_n$ and L-molecules such as ethylenediamine and 1,4-diaminebutane were implemented to synthesize monomeric complexes such as PcCo(et)CN and PcCo(bu)CN. On the other hand, [PcCoCN]$_n$ with 1,12-diaminedodecane and 2,6-diamineanthraquinone lead to PcCo(do)$_2$ and PcCo(an)$_2$ complexes. The thermal evaporation process used to produce thin film samples with these complexes does not change the intra-molecular bonds, suggesting that the deposition process has a molecular nature and the substrate temperature is not high enough to provide the surface mobility necessary for the molecular units to produce crystalline films. It was verified that the diverse molecular systems produced notable differences in their physical, spectroscopic and optical properties; here, importance has been given to the optical and electrical measurements of film samples in order to provide useful experimental data for potential applications of these kinds of compounds. Results of these measurements were carefully analyzed and discussed in order to find physical correlations and interconnections of the observed experimental data.

Concretely, the lowest electrical conductivity was found for the PcCo(an)$_2$ compound, whereas the other compounds exhibit a semiconductor behavior. The PcCo(do)$_2$ compound shows electrical conductivity values within the reported intervals found

in the literature for molecular semiconductors (from 10^{-6} to $10^{1}\ \Omega^{-1}\ cm^{-1}$). The value of the calculated activation energies and the order of magnitude of the electrical conductivities suggest that it may be possible to use of $PcCo(do)_2$ in the preparation of electronic devices. Particularly, outstanding cubic NLO effects were measured in the film samples fabricated with these materials, in both Z-Scan and THG experiments. In fact, extraordinarily huge γ-values in the order of 10^{-1} esu (for Z-Scan) and within the promising range of 10^{-11} esu (THG), were found for the developed materials. In addition to the distinctive differences provoked by the diverse chemical structures and their corresponding spectroscopic and optical properties, another correlation attributed to the thin film morphological structures (variations of the rugosity and grain sizes) could also be established; such correlations were sensitively detected and verified by NLO measurements. In fact, despite the observed differences in the film thicknesses, the surface film structures may also play an important role concerning the origin and magnitude of the observed NLO signals, as it was observed that the most NLO-efficient CN-based films exhibited the smaller grain sizes and rms rugosity, producing the higher Z-Scan and THG nonlinearities. The NLO effects agree reasonably well with the electric charge transport and conductivity measurements.

Acknowledgments

We are grateful to J. Guadalupe Bañuelos (CCADET-UNAM) for valuable support on AFM-imaging and to Dr. Neil Bruce for English revision of the manuscript. This work was supported by SEP-CONACyT-MEXICO (under grants: U-49846F, 102401and 82808).

References

[1] M.E. Sánchez-Vergara, A. Ortiz Rebollo, J.R. Alvarez, M. Rivera, J. Phys. Chem. Solids 69 (2008) 1.
[2] G.A. Kumar, G. Jose, V. Thomas, N.V. Unnikrishnan, V.P.N. Nampoori, Spectrochim. Acta A 59 (2003) 1.
[3] R.A. Collins, K.A. Mohammed, J. Phys. D: Appl. Phys. 21 (1988) 154.
[4] D. Gu, Q. Chen, J. Shu, X. Tang, G. Fuxi, S. Sten, K. Liu, X. Xu, Thin Solid Films 257 (1995) 88.
[5] T. Inabe, T.J. Marks, R.L. Burton, J.W. Lyding, W.J. McCarthy, C.R. Kannewurf, G.M. Reisner, R.H. Herbestein, Solid State Commun. 54 (1985) 501.
[6] O. Bekaroglu, Appl. Organomet. Chem. 10 (1996) 605.
[7] N.B. McKeown, J. Mater. Chem. 10 (2000) 1979.
[8] M.E. Sánchez-Vergara, I.F. Islas Bernal, M. Rivera, A. Ortíz Rebollo, J.R. Alvarez Bada, Thin Solid Films 515 (2007) 5374.
[9] M. Hanack, Inorg. Organomet. Polym. II 572 (1994) 472.
[10] S. Hünig, J. Mater. Chem. 5 (1995) 1469.
[11] T. Inabe, Y. Maruyama, Bull. Chem. Soc. Jpn. 63 (1990) 2273.
[12] M.E. Sánchez-Vergara, M.A. Ruíz Farfán, J.R. Álvarez, A. Ponce Pedraza, A. Ortiz, C. Álvarez Toledano, Spectrochim. Acta A 66 (2007) 561.
[13] J. Metz, M. Hanack, J. Am. Chem. Soc. 105 (1983) 828.
[14] A.A. Rodríguez-Rosales, O.G. Morales-Saavedra, C.J. Román, R. Ortega-Martínez, Opt. Mater. 31 (2008) 350.
[15] O.G. Morales-Saavedra, G. Huerta, R. Ortega-Martinéz, L. Fomina, J. Non-Cryst. Solids 353 (2007) 2557.
[16] P.D. Maker, R.W. Terhune, M. Nisenoff, C.M. Savage, Phys. Rev. Lett. 8 (1962) 21.
[17] H.Y. Zhang, X.H. He, Y.H. Shih, M. Schurman, Z.C. Feng, R.A. Stall, Appl. Phys. Lett. 69 (1996) 2953.
[18] N.A. Sanford, A.V. Davydov, D.V. Tsvetkov, A.V. Dmitriev, S. Keller, U.K. Mishra, S.P. DenBaars, S.S. Park, J.Y. Han, R.J. Molnar, J. Appl. Phys. 97 (2005) 053512.
[19] S. Kumar, R. Malhotra, K.S. Dhindsa, Polyhedron 11 (1992) 1383.
[20] L. Katovic, T. Taylor, D. Busch, Inorg. Chem. 3 (1971) 458.
[21] O.G. Morales-Saavedra, M.E. Sánchez-Vergara, A. Ortiz Rebollo, R. Ortega-Martínez, J. Phys. Chem. Solids 68 (2007) 1571.
[22] K. Tokumaru, J. Porph. Phthal. 5 (2001) 77.
[23] J. Simon, F. Tournillac, New J. Chem. 11 (1997) 383.
[24] J. Simon, New J. Chem. 10 (1986) 295.
[25] A.J. Jircitano, K.B. Merters, Inorg. Chem. 22 (1983) 1828.
[26] E. Ortí, Synth. Met. 33 (1989) 27.
[27] M. Dreben, M. Hanack, A. Hirsch, R. Thies, Synth. Met. 41–43 (1991) 2609.
[28] M. Sheik-Bahae, A.A. Said, E.W. Van Stryland, Opt. Lett. 14 (1989) 955.
[29] M. Sheik-Bahae, A.A. Said, D.J. Hagan, M.J. Soileau, E.W. Van Stryland, Opt. Eng. 8 (1991) 1228.
[30] M. Sheik-Bahae, A.A. Said, T. Huei Wei, D.J. Hagan, E.W. Van Stryland, IEEE J. Quantum Electron. 26 (1990) 760.
[31] T Xia, D.J. Hagan, M. Sheik-Bahae, E.W. Van Stryland, Opt. Lett. 19 (1994) 317.
[32] H.S. Nalwa, S. Miyata (Eds.), Nonlinear Optics of Organic Molecules and Polymers., CRS Press Inc, Boca Raton, FL, 1997.
[33] C.Y. Liu, B.P. Zhang, N.T. Binh, Y. Segawa, Opt. Commun. 237 (2004) 65.
[34] L. Castañeda, O.G. Morales-Saavedra, D.R. Acosta, M.L. Olvera, A. Maldonado, Phys. Stat. Sol. A 203 (2006) 1971.
[35] J. Khaled, T. Fujiwara, M. Ohama, A.J. Ikushima, J. Appl. Phys. 87 (2000) 2137.
[36] U. Neuman, R. Grunwald, U. Griebener, G. Steinmeyer, Appl. Phys. Lett. 84 (2004) 170.
[37] F. D'Amore, A. Zappettini, G. Facchini, S.M. Pietralunga, M. Martinelli, C. Dell'Erba, C. Cuniberti, D. Comoretto, G. Delle piane, Synth. Met. 127 (2002) 143.
[38] F. D'Amore, M. Di Giulio, S.M. Pietralunga, A. Zappettini, L. Nasi, V. Rigato, M. Martinelli, J. Appl. Phys. 94 (2003) 1654.
[39] H. Nakanishi, H. Matsuda, S. Okada, M. Kato, Polym. Adv. Technol. 1 (1990) 75.
[40] B. Buchalter, G.R. Meredith, Appl. Opt. 21 (1982) 3221.
[41] G.R. Meredith, Phys. Rev. B 24 (1981) 5522.
[42] X.H. Wang, D.P. West, N.B. McKoewn, T.A. King, J. Opt. Soc. Am. B 15 (1998) 1895.
[43] K. Miyano, T. Nishiwaki, A. Tomioka, Opt. Commun. 91 (1992) 501.
[44] D.S. Bethune, J. Opt. Soc. Am. B 6 (1989) 910.